Wall to wall stress induced on (6,5) semiconducting nanotubes by encapsulation in metallic outer tubes of different diameters: A Resonant Raman Study of individual C_{60}-derived double wall carbon nanotubes

F. Villalpando-Paez[1] , H. Muramatsu[2,3], Y.A. Kim[2,3], M. Endo[2,3], M. Terrones[4], M.S. Dresselhaus[5,6]
[1]*Department of Materials Science and Engineering, Massachusetts Institute of Technology, Cambridge, MA. 02139-4307,USA.*
[2]*Institute of Carbon Science and Technology, Shinshu University, 4-17-1 Wakasato, Nagano-shi 380-8553, Japan*
[3]*Faculty of Engineering, Shinshu University 4-17-1 Wakasato, Nagano-shi 380-8553, Japan.*
[4]*Laboratory for Nanoscience and Nanotechnology Research (LINAN) and Advanced Materials Department, IPICYT, San Luis Potos, 78216, Mxico. and*
[5,6]*Department of Physics and Department of Electrical Engineering and Computer Science, Massachusetts Institute of Technology, Cambridge, MA. 02139-4307,USA.*
(Dated: September 7, 2009)

We measure resonant Raman scattering from 11 individual C_{60}-derived double wall carbon nanotubes with inner semiconducting (6,5) tubes and outer metallic tubes. The Raman spectra show the radial breathing mode (RBM) of the inner and the outer tubes simultaneously in resonance with the same laser energy. We observe that an increase in the RBM frequency of the inner tubes is related to an increase in the RBM frequency of the outer tubes. The Raman spectra also contain a sharp G^- feature that increases in frequency as the nominal diameter of the outer metallic tubes decreases. Finally, the one phonon second-order D band mode shows a two way frequency splitting that decreases with decreasing nominal wall to wall distances. We suggest that the stress which increases with decreasing nominal WtW distances is responsible for the observed hardening of the frequencies of the RBM, D an G^- modes of the inner (6,5) semiconducting tubes.

I. INTRODUCTION

Double wall carbon nanotubes (DWNTs) exhibit optical and vibrational properties that are similar to those of single wall carbon nanotubes (SWNTs) but their double wall structure makes them more mechanically and thermally robust [1]. Depending on the metallic (M) or semiconducting (S) nature of their inner and outer tubes, DWNTs can have four possible configurations, S@S, S@M, M@S, M@M, each of which is expected to have particular properties suitable for different electronic device applications.

Possible techniques for fabricating DWNTs include chemical vapor deposition (CVD) [1, 2] or the filling of SWNTs with fullerenes that coalesce and form inner tubes upon heat treatment [3, 4]. Both types of DWNTs are studied in the present work and are inter-compared. In the case of C_{60}-derived DWNTs (denoted by C_{60}-DWNTs), the coalescence of fullerenes at high temperature (>1200°C) forms inner tubes with diameters (d_t) close to that of C_{60} [4]. According to Bandow et al., under prolonged heat treatments the initial diameters of the inner tubes can increase in order to adjust the wall to wall (WtW) distances and minimize the energy of the system [4]. Also, by using high resolution Raman spectroscopy, Pfeiffer *et al.* [5–8] and Kuzmany *et al.* [9], observed that the inner tubes of C_{60}-DWNTs can be contained inside outer tubes with different diameters where smaller WtW distances increase the inter-tube interaction and upshift the RBM of the inner tubes. CVD-DWNTs and C_{60}-DWNTs have been shown to have different optical properties that are believed to originate from differences in the WtW distances and the degree of crystallinity of the inner tubes. For instance, on one hand, a quenching of the photoluminescence (PL) signal has been observed in C_{60}-DWNTs and attributed to inter-tube interactions [10]. On the other hand, in CVD-DWNTs, a strong PL from the inner semiconducting tubes has been recently observed [11].

To the best of our knowledge, most spectroscopic experiments on DWNTs have been performed on bundles or solution-based samples, so that it has been inherently difficult to use Raman spectra to investigate which inner (n,m) tubes are actually contained inside the variety of observed outer (n',m') tubes. In order to quantitatively determine which specific inner and outer tubes actually form each DWNT, one must perform experiments on individual DWNTs [12]. Therefore, in the present work individual C_{60}-DWNTs have been dispersed on a substrate and studied independently. Here we report a brief comparison between CVD-DWNT and C_{60}-DWNT bundles and a detailed study of 11 individual isolated C_{60}-DWNTs with inner semiconducting (6,5) tubes and outer metallic tubes.

II. EXPERIMENTAL DETAILS

We used a CVD method to synthesize the CVD-DWNT bundles used in this study. The high purity of our CVD-DWNT bundles relative to residual catalyst particles and SWNTs has been confirmed by diamagnetic susceptibility [13, 14] and Raman spectroscopy experiments [15], respectively. The C_{60}-DWNT bundles used herein were fabricated by reacting C_{60} and SWNTs under vacuum at 600°C for 24h. The starting SWNT material

was synthesized by the arc method and purified by Hanwha Corp (Korea). The as-grown peapods were washed with toluene to remove residual C_{60} and heat treated at 1700°C in Ar (1 atm) to transform them into C_{60}-DWNT bundles. A high resolution transmission electron micrograph (HRTEM) of the resulting C_{60}-DWNT material is shown in Fig. 1(a). The solution containing isolated C_{60}-DWNTs was prepared by dispersing 1mg of C_{60}-DWNTs in D_2O with 0.5 wt.% sodium dodecilbenzenesulfonate (SDBS) and sonicating the dispersion (600 W/cm^2) for 15-30 min. Subsequently, the solution was ultracentrifuged (320,000 g) for 30min and 70% of the supernatant solution was collected. A PL map from the resulting C_{60}-DWNT solution shows (see Fig. 1(b)) the presence of three (n,m) species where the strongest peak corresponds to (6,5) semiconducting tubes.

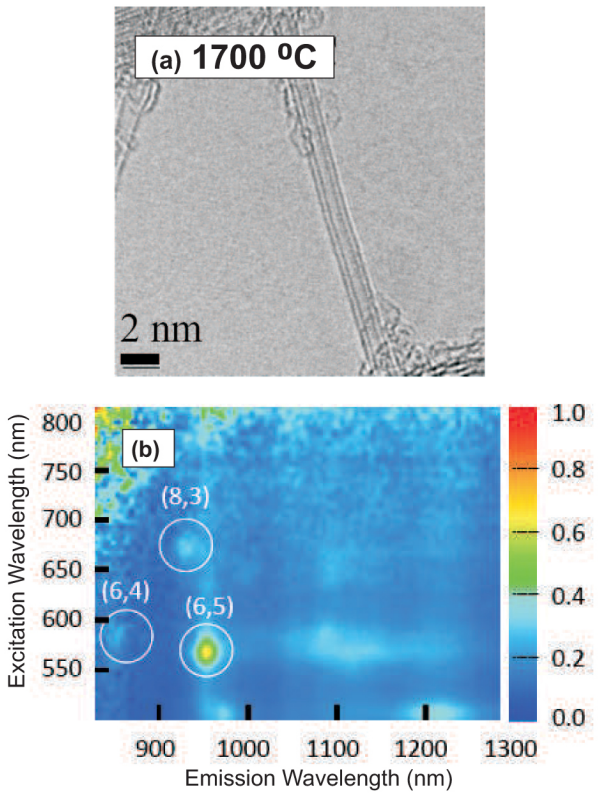

FIG. 1: (a) HRTEM of a C_{60}-DWNT produced by heat treating peapods at 1700°C in Ar (b) Photoluminescence (PL) map of a solution containing isolated C_{60}-DWNTs dispersed in sodium dodecilbenzenesulfonate (SDBS). The strongest PL peak corresponds to semiconducting (6,5) inner tubes.

The solution containing isolated C_{60}-DWNTs was spin-coated on a silicon substrate that is marked with a gold grid and allows for precise recording of the location of an isolated DWNT (see inset of Fig. 2(b)) [12]. The distribution of the deposited DWNTs on the silicon substrate is not spatially homogeneous but the nanotube density is low enough to have 0 to 20 nanotubes per $100\mu m^2$. The laser spot has a $1\mu m$ diameter and, depending on its location on the substrate, the laser spot illuminated 0 to 5 DWNTs. For bundles, 5 measurements were performed on different spots and laser power levels were kept below 0.5mW to avoid excessive heating. Scattered light was collected through a 100X objective using a backscattering geometry. An Nd:YAG laser was used to generate E_{laser}=2.33eV and a Kr^+ ion laser generated E_{laser} =1.92eV. A dye laser containing Rhodamine 6G dye and a Ti:sapphire laser were pumped by the Nd:YAG laser to generate E_{laser}=2.05-2.16eV and E_{laser} =1.6eV, respectively. A thermoelectrically-cooled Si CCD (charge coupled device) detector operating at -75°C was used to collect spectra.

In order to obtain a strong Raman signal from an isolated carbon nanotube, the resonance condition must be met by matching the laser energy to the energy separation between the van Hove singularities of the isolated nanotube [16]. Our laser spot often illuminates nanotubes that are not in resonance with the laser energy. Therefore, in order to find resonant nanotubes with a strong radial breathing mode (RBM) Raman signal, we scanned large substrate areas ($900\mu m^2$).

III. RESULTS AND DISCUSSION

A. Bundle DWNTs

Before starting the discussion on individual C_{60}-DWNTs, we briefly comment on the RBM spectra of our C_{60}-DWNT and CVD-DWNT bundles. As shown in Fig. 2(a), and in agreement with a previous report [8], C_{60}-DWNTs have a narrower d_t distribution than CVD-DWNTs. This observation was expected because, in the case of C_{60}-DWNTs, the d_t distribution of the starting SWNT material limits the possible choice of d_t for the inner tubes when the fullerenes coalesce through heat treatment. In the case of CVD-DWNTs, this d_t limitation is not present and, when using E_{laser}=2.13eV, we find resonance with semiconducting tubes for 8 different diameters and metallic tubes with d_t=1.41 and 0.97nm (see Fig. 2(a)). As is expected, the RBM frequencies of the inner and outer tubes of the individual C_{60}-DWNTs that we study in the following section, coincide with the RBM frequencies of the most prominent tube diameters observed in the C_{60}-DWNT bundles (See vertical lines connecting the shaded Lorentzians in Fig. 2 (a) to the RBM pair in Fig. 2 (c)).

B. Isolated, Individual C_{60}-DWNTs

Herein we describe the procedures that allowed us to detect isolated C_{60}-DWNTs and we then discuss the

dependence of the ω_{RBM}, ω_{G^-} and ω_D frequencies on DWNT nominal inner tube diameter and WtW distance.

After studying the large area Raman maps of the Si substrate, on a few occasions ($\sim$<5%), it was possible to find locations on the Si substrate that showed two RBM modes, simultaneously in resonance with the same E_{laser}. These pairs of RBMs come from two nanotubes, one with a small diameter ($\sim$0.7nm) and another one with a large ($\sim$1.3nm) diameter. The observation of these RBM pairs (see Fig. 2(c)) suggested that we had found a resonance with the inner and outer tubes of the same DWNT. However, although the probability is low, a rope of 2-3 DWNTs could also generate a pair of RBMs if the inner and outer tubes of two different DWNTs happen to be in resonance with the same E_{laser}. Therefore, in order to confirm that the two observed RBMs were indeed coming from the same DWNT, we verified that only one DWNT was being illuminated by the laser spot. This verification consisted of three steps whose results are shown, for the same DWNT, in Fig. 2:

(1) We used AFM (atomic force microscopy) to check that the DWNT is completely isolated and far away from the other tubes on the substrate (See Fig. 2(b)). The inset in Fig. 2(b) shows the Au grid used to mark and record the location of each individual DWNT.

(2) We checked that the height of the DWNT as measured by AFM corresponds to the diameter of the outer tube of the DWNT as deduced from its low frequency RBM. Figure 2(d) shows the AFM height profile of our DWNT. The difference between the measured Raman and AFM outer tube diameter estimates is $\sim$0.1nm.

(3) Finally we scan the same spot in the sample with multiple laser lines in order to eliminate the presence of additional nanotubes that might not have been in resonance with the initial laser energy. Figure 2(c) shows the RBM region of the Raman spectrum coming from one isolated DWNT taken with E_{laser}=2.11eV. The same spot on the substrate was also scanned with 9 different laser energies (2.33, 2.16, 2.14, 2.12, 2.10, 2.07, 2.05, 1.92 and 1.60 eV) and no additional RBMs coming from other nanotubes were detected.

Performing AFM and acquiring Raman spectra with many E_{laser} on isolated DWNTs is feasible [12] but also experimentally challenging. While attempting to increase the throughput of the above mentioned technique, we discovered that it is also possible to use less AFM time and only one laser line and still be almost certain that we are in resonance with the inner and outer tubes of the same DWNT. We now describe a new procedure that allowed us to detect 11 isolated C_{60}-DWNTs.

First we used one laser line (2.08 or 2.10eV) to find as many spectra as possible containing two simultaneous RBMs (see Fig. 3) that matched the expected inner and outer tube diameters of the individual DWNTs present in our sample (see Fig. 4). By plotting the low frequency RBM (large diameter tubes) vs high frequency RBM (small diameter tubes) for each spectrum, we found that the frequencies of most of the simultaneously detected RBM pairs (80%) were correlated (see Fig. 5(a)). We know *a priori* that if the two simultaneously resonant RBMs do not correspond to the same DWNTs we should observe random low frequency RBM vs high frequency RBM relationships. Therefore, the trend followed by the simultaneous RBM pairs plotted in Fig. 5(a) suggests that each RBM pair is indeed coming from the inner and outer tubes of a single isolated DWNT. Thus, if the observed pair of RBMs fits the trend in Fig. 5(a), then the pair is identified as most likely coming from the same isolated DWNT and the pair is then retained; otherwise the spectra are discarded in this analysis.

The Kataura plot in Fig. 3 shows that, when using E_{laser}=2.08 and 2.10eV, we excited the E_{22}^S transitions of (6,5) inner semiconducting tubes and the E_{11}^M transitions of outer metallic tubes mainly from family 2n+m=33. The Kataura plot was calculated within the ETB (extended tight binding) framework [17], including many-body corrections, fitted to the RRS (resonance Raman scattering) data from sodium docecyl sulfate-wrapped HiPCO (High Pressure CO conversion) SWNTs [18]. We find that such a Kataura plot (Fig. 3) which is based on prior studies on SWNTs [17], is accurate enough for the qualitative identification of the (n,m) assignment for small diameter tubes within DWNTs. Although the relationship between ω_{RBM} and d_t for the inner tubes and outer tubes of DWNTs is not expected to be the same as it would be for isolated SWNTs, we approximate the nanotube diameters for both the inner and outer tubes of DWNTs in this work by using the SWNT-based RBM relation $\omega_{RBM} = 218.3/d_t + 15.9$ [14], because there are no experimental or theoretical ω_{RBM} vs d_t relationships presently available for the inner and outer tubes that constitute the four different kinds of DWNT configurations (S@S, S@M, M@S, M@M) as mentioned above. Also, nanotube-substrate van der Waals interactions are known to induce radial deformations that can upshift the ω_{RBM} of large diameter SWNTs [19]. However, in this work we assume that nanotube-substrate interactions have a negligible effect on the ω_{RBM} of each of the two layers of our DWNTs because (a) the d_t of the outer tubes is relatively small (1.3nm), (b) the deformation of the outer tube is reduced by the presence of the inner tube and (c) because, to a first order approximation, the inner tube is shielded and not affected by the substrate.

Based on the SWNT-based RBM relation mentioned above, we find that the ω_{RBM} values for the 11 DWNT specimens experimentally measured in this work yield nominal inner (outer) tube diameters in the 0.69-0.73nm (1.28-1.35nm) range. The nominal WtW distances for these 11 C_{60}-DWNTs are calculated by subtracting the nominal d_t of the inner tubes from the nominal d_t of the outer tubes obtained by the above procedure, yielding nominal WtW distances in the 0.58-0.65nm range. In Fig. 5(a) we plot the measured ω_{RBM} of each inner tube vs. the ω_{RBM} of its corresponding outer tube for the 11 measured tubes. All the inner tubes in this work are assigned to (6,5) nanotubes and we observe that their

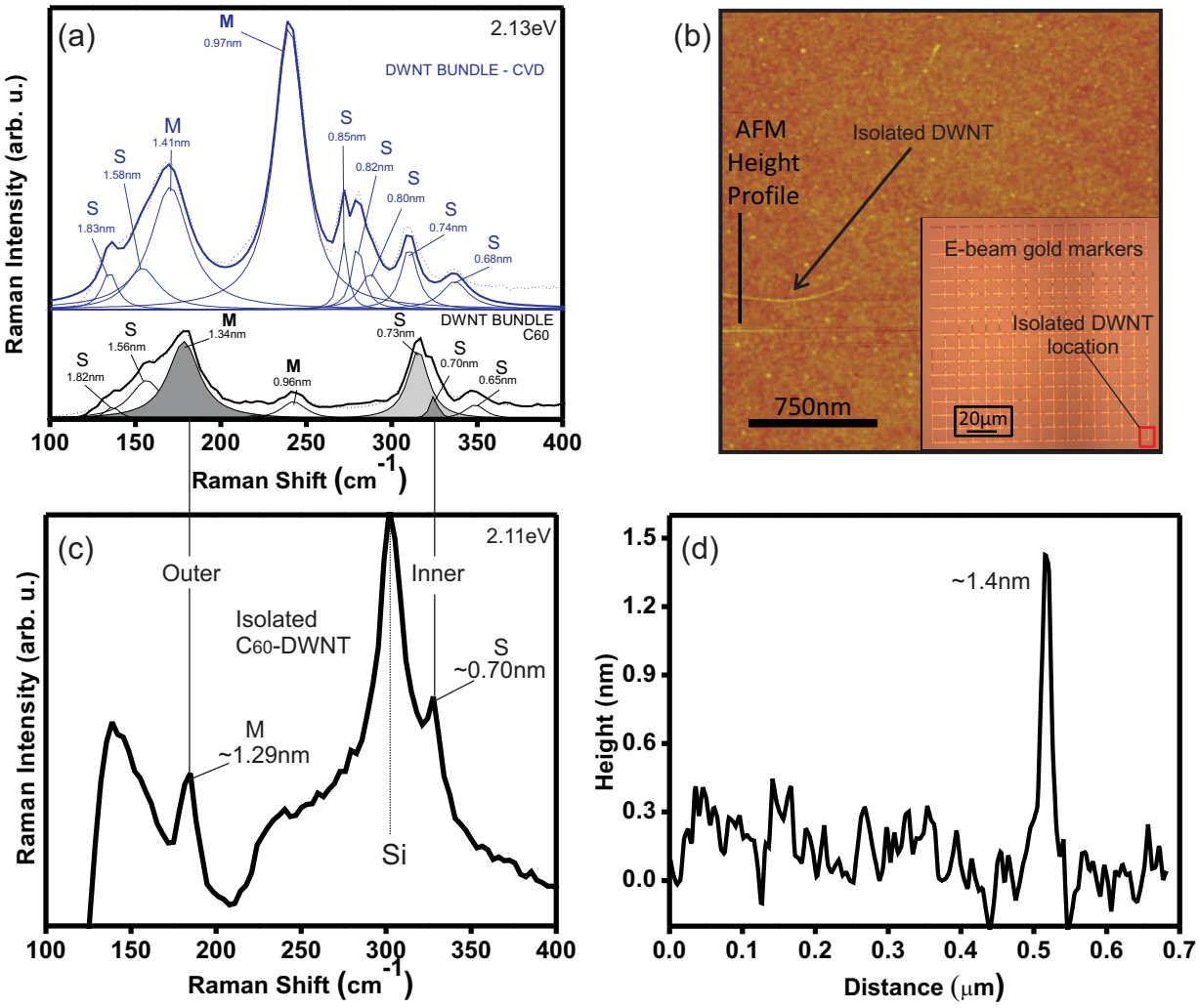

FIG. 2: (a) Raman spectra for the RBM region for CVD-DWNT and C_{60}-DWNT bundles (E_{laser}=2.13eV). (b) Atomic Force Microscope (AFM) image of one individual, isolated DWNT. Inset: Silicon substrate with Au markers showing the location of the DWNT. (c) Raman spectra for the RBM Raman region (E_{laser}=2.11eV) for an isolated individual C_{60}-DWNT and (d) Atomic Force Microsope (AFM) height profile of the individual, isolated DWNT shown in (b) with the RBM spectrum shown in (c). The vertical lines connecting (a) and (c) show that the ω_{RBM} of the prominent tube diameters observed in the C_{60}-DWNT bundles coincide with the ω_{RBM} of the inner and outer tubes of the isolated C_{60}-DWNTs.

measured ω_{RBM} values upshift with increasing measured outer tube ω_{RBM} values (Fig. 5(a)). Similarly, the measured ω_{RBM} of the inner tubes upshift with decreasing nominal WtW distance as shown in Fig. 5(b) and in qualitative agreement with the results in Refs. [5–9].

Because of the strong carbon-carbon bond and their small d_t, we do not expect the actual diameter of the inner tubes to decrease to the values given by the SWNT-based RBM relation. Instead, the observed hardening of the measured ω_{RBM} as the nominal WtW distance decreases corresponds to a minimal change in actual inner tube d_t and provides an indirect measure of the stress that is felt by the inner tube. All the eleven inner tubes shown herein are Type II semiconducting (6,5) tubes but the outer tubes that surround them vary somewhat in diameter and can be identified with a few different (n,m) values from one another, but certainly far less than 11 different values.

1. *Dependence of ω_{G^-} on inner tube ω_{RBM} and wall to wall (WtW) distance.*

The tangential G-band modes in carbon nanotubes can be TO (transverse optic) and LO (longitudinal optic). The frequencies of the LO and TO modes vary with the

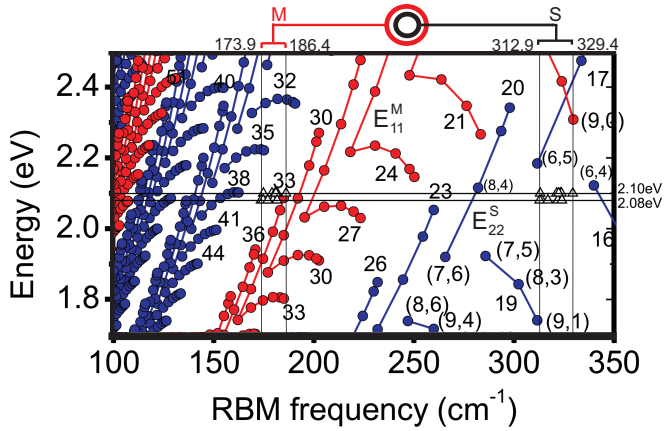

FIG. 3: Kataura plot of the resonant transition energies vs. RBM frequencies for SWNTs based on the extended tight binding model [17]. The location on the plot of the measured DWNT RBMs are marked with triangles. The laser energies (2.08 and 2.10 eV) chosen to excite DWNTs with inner semiconducting and outer metallic tubes are marked with horizontal lines. The vertical lines denote the ranges of ω_{RBM} measured for the inner and outer tubes.

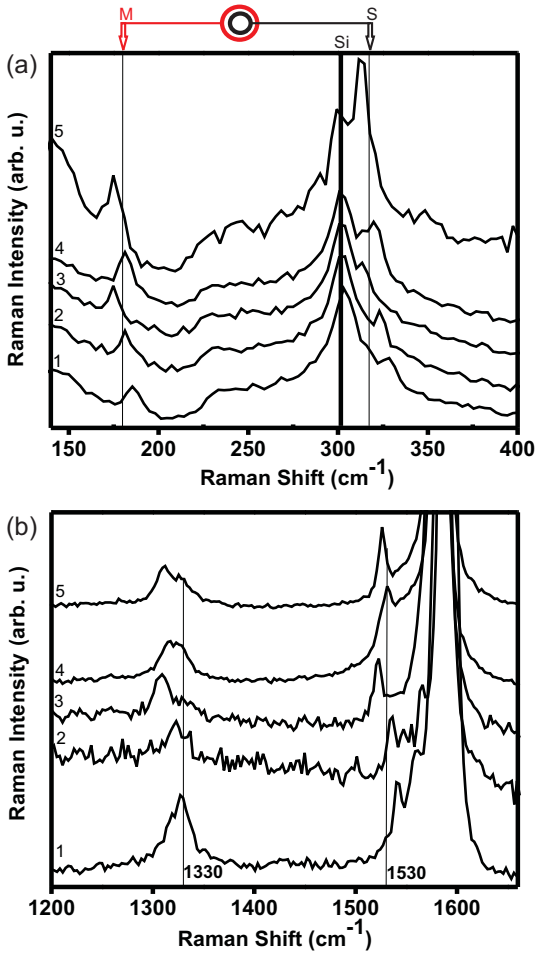

FIG. 4: (a) RBM-band and (b) D-band and G-band regions of the Raman spectra corresponding to five different DWNTs whose inner and outer walls are simultaneously in resonance with the same laser line E_{laser}= 2.10eV. Vertical lines in (a) denote outer M tubes and inner S (6,5) tubes and the dark vertical line denotes a Si Raman feature. The vertical lines in (b) denote D-band and G-band features (see text).

degree of confinement, curvature and chiral angle of each particular (n,m) nanotube and the intensities of the TO and LO modes are sensitive to the angle formed between the nanotube axis and the polarization of the incoming light [20]. For semiconducting nanotubes, the LO mode (G^+ band) is a bond stretching mode with little diameter dependence and the TO mode is a bond bending mode whose frequency decreases with decreasing nanotube diameter (G^- band) [21]. Also, the G^- band of isolated semiconducting tubes (S-SWNTs) generally has a smaller FWHM linewidth than that of metallic tubes [22].

Since the inner tubes of our DWNTs are semiconducting, their spectra show sharp G^- features that are easy to fit unambiguously with a Lorentzian lineshape. If we correlate ω_{G-}, the frequency of the G^- band, to the low frequency RBM (corresponding to the inner tube) in our spectra for DWNTs, we observe an increase in ω_{G-} as ω_{RBM} for the inner nanotube increases (see Fig. 5(c)). This behavior is opposite to the well-documented diameter dependence of the G^- (LO) mode in S-SWNTs [16].

We explain this observation in the following way. We know from Fig. 5(b) that DWNTs whose inner tube show an upshifted ω_{RBM} tend to have smaller nominal WtW distances. A smaller nominal WtW distance implies a higher degree of inter-tube interaction and a higher stress felt by both the inner and outer tubes of an individual DWNT. Therefore, we expect the observed hardening of the G^- frequency with increasing inner tube ω_{RBM} (see Fig. 5(c)) to be caused by the increased stress that the outer and inner tubes exert on each other in the case of DWNTs as the WtW distances decrease. Experimentally, although not shown explicitly in this work, the intensity of the G^- band is not observed to show any significant dependence on the nominal WtW distance.

Finally, we expect the G^+ region of our DWNTs to contain a contribution from the LO mode of its S inner tube and the TO mode of its M outer tube. Unfortunately, the G^+ of the inner tubes and the G^+ of the outer tubes from our DWNTs overlap so that we can not distinguish the separate contributions made by each of the tubes and we were not able to study possible correlations between G^+ frequency and the ω_{RBM} of the inner nanotube.

2. *Dependence of ω_D on inner tube ω_{RBM} and wall to wall (WtW) distance.*

The D band is a one-phonon second-order band that appears when the translational symmetry of a nanotube

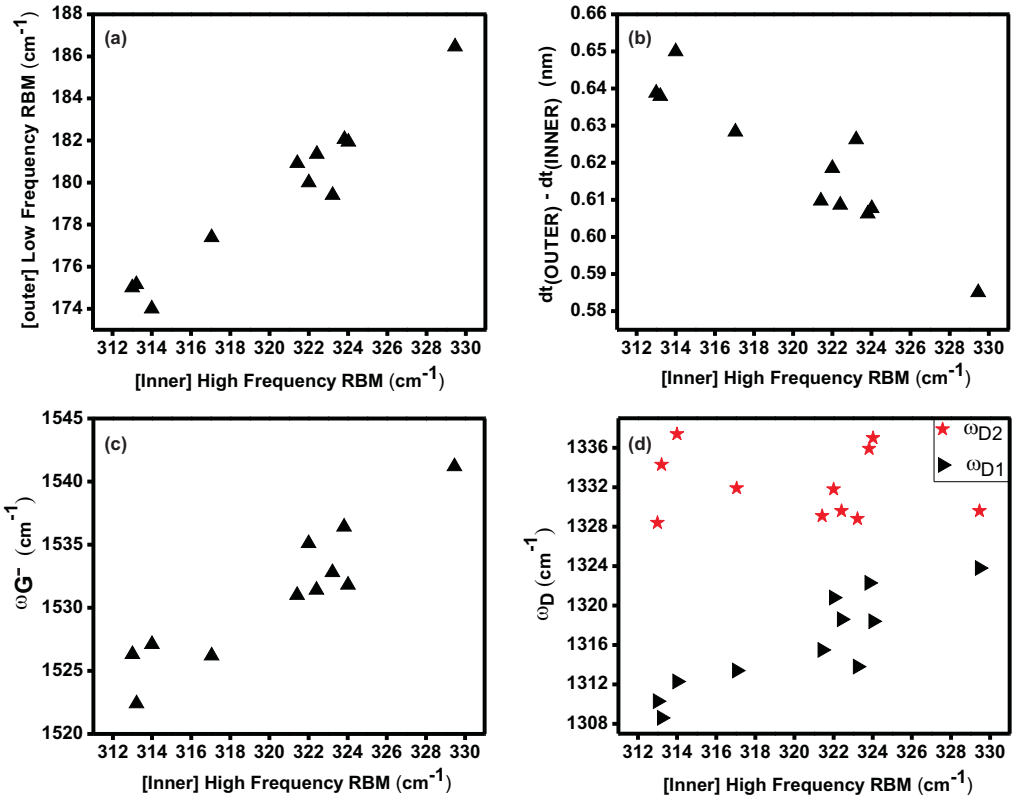

FIG. 5: (a) Correlation between the ω_{RBM} of the inner and outer tubes of the same C_{60}-DWNT. All the inner tubes for the 11 C_{60}-DWNTs in this figure are (6,5) tubes. (b) Correlation between the WtW distance of each DWNT with ω_{RBM} for its inner tube. An increase in the ω_{RBM} of the inner tubes is accompanied by a decrease in the nominal WtW distance. (c) Plot of ω_{G^-} vs ω_{RBM} for the inner tube of each DWNT. An upshift in ω_{G^-} results from a decrease in the nominal WtW distance and increased inter-tube interaction. (d) The ω_{D1} for each component of the D-band vs ω_{RBM} for the inner tube of each of the 11 DWNTs. The splitting of the D-band into ω_{D1} and ω_{D2} decrease as ω_{RBM} of the inner tube increases with decreasing nominal WtW distance. Note that ω_{D2} remains almost constant while ω_{D1} increases.

is broken. In the case of SWNTs, the D band can be fit with one Lorentzian and, like the G^- mode, the D band softens with decreasing nanotube diameter [16]. The lineshape of the observed D band from our DWNTs (see Fig. 4 (b)) can be fit with one low (ω_{D1}) and one high (ω_{D2}) frequency Lorentzian which can be correlated with the inner (lower frequency) and outer (higher frequency) tubes of each DWNT. A factor that contributes to the splitting of the D-band in this collection of DWNTs is the diameter dependence of ω_D which makes the splitting more evident for larger nominal WtW distances between inner and outer tubes (see leftmost part of Figs. 5(b) and (d)). As shown in Fig. 5(d), we observe that when the ω_{RBM} of the inner tube increases, ω_{D1} upshifts, probably due to a decreased WtW distance that results in an increasingly stressed inner tube. Finally, although not shown explicitly in this work, the intensity of the D-band components (D1 and D2) do not show a dependence on the ω_{RBM} of the inner tube.

IV. CONCLUSIONS

In this work we obtained the Raman spectra of 11 isolated C_{60}-DWNTs all with inner semiconducting (6,5) tubes but with different outer metallic tubes by searching for RBM pairs that were simultaneously in resonance with the same E_{laser} and that matched the expected inner and outer tube diameters of individual DWNTs. In this collection of isolated C_{60}-DWNTs we observed that the ω_{RBM} of the inner (6,5) semiconducting tube hardens as the diameter of the outer metallic tube decreases. We also measured an increase in ω_{G^-} with decreasing wall to wall distances and attributed the upshift of ω_{G^-} to the stress felt by the inner tubes of the DWNTs due to increasing inter-tube interaction. Finally, we noted that the D band mode splits into two components where the lower frequency component ω_{D1} is related to the inner tube and hardens with decreasing nominal WtW distances. The upper frequency D-band component ω_{D2} related to the outer tube is independent of the nominal WtW distance. In the future we expect to use the same

technique to find specimens with the remaining three DWNT configurations and compare their optical properties as the intertube distances are varied.

Acknowledgments

The authors gratefully acknowledge financial support from CONACYT Mexico: 56787 (Laboratory for Nanoscience and Nanotechnology Research-LINAN), 45772 (M.T.), 58899-Inter American Collaboration (M.T.), the MIT-CONACYT program (M.S.D., M.T.), 2004-01-013/SALUD-CONACYT(M.T.). We also thank CONACYT graduate student grants, Vilore Foods Co. and SEP Mexico for financial support (F.V.P). The authors M.E., Y.A.K and H.M. acknowledge support from the CLUSTER project (second stage) and a grant for Specially Promoted Research (No. 19002007) from the Ministry of Education, Culture, Sports, Science and Technology of Japan. The authors F.V.P., and M.S.D. gratefully acknowledge support from NSF/DMR 07-04197. The authors are grateful to D. Nezich for providing marked Si substrates and to H. Farhat, A.Reina, M. Hofmann, E. Barros, A.G. Souza and L.G. Cancado for helpful discussions.

[1] Y. A. Kim, H. Muramatsu, T. Hayashi, M. Endo, M. Terrones, and M. S. Dresselhaus, Chemical Physics Letters **398**, 87 (2004).
[2] M. Endo, H. Muramatsu, T. Hayashi, Y. A. Kim, M. Terrones, and N. S. Dresselhaus, Nature **433**, 476 (2005).
[3] S. Bandow, M. Takizawa, H. Kato, T. Okazaki, H. Shinohara, and S. Iijima, Chemical Physics Letters **347**, 23 (2001).
[4] S. Bandow, T. Hiraoka, T. Yumura, K. Hirahara, H. Shinohara, and S. Iijima, Chemical Physics Letters **384**, 320 (2004).
[5] R. Pfeiffer, C. Kramberger, F. Simon, H. Kuzmany, V. N. Popov, and H. Kataura, European Physical Journal B **42**, 345 (2004).
[6] R. Pfeiffer, F. Simon, H. Kuzmany, and V. N. Popov, Physical Review B **72**, 161404 (2005).
[7] R. Pfeiffer, F. Simon, H. Kuzmany, V. N. Popov, V. Zolyomi, and J. Kurti, Physica Status Solidi B-Basic Solid State Physics **243**, 3268 (2006).
[8] R. Pfeiffer, H. Peterlik, H. Kuzmany, F. Simon, K. Pressi, P. Knoll, M. H. Rummeli, H. Shiozawa, H. Muramatsu, Y. A. Kim, et al., Physica Status Solidi B-Basic Solid State Physics **245**, 1943 (2008).
[9] H. Kuzmany, W. Plank, R. Pfeiffer, and F. Simon, Journal of Raman Spectroscopy **39**, 134 (2008).
[10] T. Okazaki, S. Bandow, G. Tamura, Y. Fujita, K. Iakoubovskii, S. Kazaoui, N. Minami, T. Saito, K. Suenaga, and S. Iijima, Physical Review B **74**, 153404 (2006).
[11] D. Shimamoto, H. Muramatsu, T. Hayashi, Y. A. Kim, M. Endo, J. S. Park, R. Saito, M. Terrones, and M. S. Dresselhaus, Applied Physics Letters **94**, 083106 (2009).
[12] F. Villalpando-Paez, H. Son, D. Nezich, Y. P. Hsieh, J. Kong, Y. A. Kim, D. Shimamoto, H. Muramatsu, T. Hayashi, M. Endo, et al., Nano Letters **8**, 3879 (2008).
[13] Y. A. Kim, H. Muramatsu, T. Hayashi, M. Endo, M. Terrones, and M. S. Dresselhaus, Chem. Vap. Deposition **12**, 327 (2006).
[14] M. Endo, Y. A. Kim, T. Hayashi, H. Muramatsu, M. Terrones, R. Saito, F. Villalpando-Paez, S. G. Chou, and M. S. Dresselhaus, Small **2**, 1031 (2006).
[15] Y. Kim, H. Muramatsu, M. Kojima, T. Hayashi, M. Endo, M. Terrones, and M. Dresselhaus, Chem. Phys. Lett. **420**, 377 (2006).
[16] M. Dresselhaus, G. Dresselhaus, R. Saito, and A. Jorio, Physics Report **409**, 49 (2005).
[17] G. G. Samsonidze, R. Saito, N. Kobayashi, A. Gruneis, J. Jiang, A. Jorio, S. G. Chou, G. Dresselhaus, and M. S. Dresselhaus, Applied Physics Letters **85**, 5703 (2004).
[18] A. Jorio, C. Fantini, M. Pimenta, R. B. Capaz, G. G. Samsonidze, M. S. Dresselhaus, N. Kobayashi, A. Gruneis, and R. Saito, Physical Review B **71**, 075401 (2005).
[19] L. Gomez-De Arco, B. Lei, S. Cronin, and C. W. Zhou, Applied Physics Letters **93**, 123112 (2008).
[20] R. Saito, A. Jorio, J. H. Hafner, C. M. Lieber, M. Hunter, T. McClure, G. Dresselhaus, and M. S. Dresselhaus, Physical Review B **6408**, 085312 (2001).
[21] P. S., L. M., R. J., F. A. C., and M. F., Physical Review B **75**, 035427 (2007).
[22] A. Jorio, A. G. Souza, G. Dresselhaus, M. S. Dresselhaus, A. K. Swan, M. S. Unlu, B. B. Goldberg, M. A. Pimenta, J. H. Hafner, C. M. Lieber, et al., Physical Review B **65**, 155412 (2002).